Tunneling Statistics for Analysis of Spin-Readout Fidelity

S. K. Gorman, Y. He, M. G. House, J. G. Keizer, D. Keith, L. Fricke, S. J. Hile, M. A. Broome, and M. Y. Simmons

Centre of Excellence for Quantum Computation and Communication Technology, School of Physics, University of New South Wales, Sydney, New South Wales 2052, Australia

(Received 4 May 2017; revised manuscript received 3 August 2017; published 22 September 2017)

We investigate spin and charge dynamics of a quantum dot of phosphorus atoms coupled to a radio-frequency single-electron transistor (SET) using full counting statistics. We show how the magnetic field plays a role in determining the bunching or antibunching tunneling statistics of the donor dot and SET system. Using the counting statistics, we show how to determine the lowest magnetic field where spin readout is possible. We then show how such a measurement can be used to investigate and optimize single-electron spin-readout fidelity.

DOI: 10.1103/PhysRevApplied.8.034019

I. INTRODUCTION

Single-shot electron spin readout is crucial for scalable quantum computation in silicon [1,2]. The single-electron transistor (SET) has proven to be a highly sensitive electron charge detector in recent years [3–5] and is routinely used to perform high-fidelity electron spin readout when operated in dc mode [6–9]. The SET can also be operated in ac mode using rf reflectometry, which has been shown to increase detection bandwidths and give larger signal-to-noise ratios (SNRs) [10–13]. However, it is not known how a rf-driving field will affect the fidelity of electron spin readout or if electron spin readout is even possible in devices where the electron is tunnel coupled to a rf SET. To investigate the combined rf SET and electron system for single-shot spin readout, we examine the statistical properties of electrons tunneling between a single donor dot (DD) comprised of approximately 5-P atoms and a rf SET.

Electron spin readout is governed by spin-selective tunneling processes of an electron from a DD to an electron reservoir [14]. In particular, the tunnel out rates of the electron spin-up and spin-down states from the DD to the reservoir need to be vastly different to ensure high-fidelity spin-to-charge conversion [8]. If the tunnel rates are too similar, they cannot be attributed to the correct qubit state. Importantly, in such a system, the tunneling statistics of electrons to and from a reservoir can provide a vast amount of information about the underlying physical processes for the coupled DD SET system [15–18]. This information can, in turn, be used to optimize the spin-readout fidelity using full counting statistics (FCS) [19–21]. In addition, FCS can be used to investigate shot noise [22,23], non-Markovian effects [24–26], and electron-electron interactions [27,28] that are difficult to obtain from transport measurements alone.

Full counting statistics involves counting the number of tunnel events n of an electron typically between a reservoir and electronic state such as a quantum dot within a time window τ [29]. By repeatedly counting the tunnel events over many multiples of τ, a number distribution of tunnel events $p(n)$ can be obtained [22]. The resulting distribution can be completely described by a set of cumulants κ_i derived from the natural logarithm of the moment-generating function of $p(n)$. The cumulants represent different statistical properties of the number distribution, in which κ_1, κ_2, and κ_3 are the mean, variance, and skewness, respectively [17,30]. Knowledge of the tunneling statistics can then be used to optimize the time and energy detuning for electron spin readout since they rely on the tunneling of electrons from the DD to the reservoir.

In this work, we show by analyzing the random telegraph signal (RTS) produced from the DD electron tunnel events how the system varies under different magnetic field and rf-power conditions. The paper is laid out in the following sections. In Sec. II, we describe the operation of the device and outline the measurement of RTS traces. We then derive the first few cumulants in terms of the electronic tunnel rates in the system in Sec. II A. We investigate the dependence of FCS on magnetic field and rf power in Sec. III, and in more detail, the low, high, and intermediate magnetic field regimes in Secs. III A–III C. In Sec. IV, we present a short overview of fidelity analysis of spin readout and discuss how to optimize the readout time in Sec. IV A, as well as the rf power of the rf SET in Sec. IV B. Finally, in Sec. V, we summarize the results and describe potential future extensions to this work.

II. DEVICE CHARACTERIZATION

The device is patterned using scanning-tunneling-microscopy (STM) hydrogen lithography to selectively remove a hydrogen mask and subsequently dose with phosphine to incorporate phosphorus donors [31]; see Fig. 1(a). The device is mounted on a printed circuit board with a rf-tank circuit that has a resonant frequency of 228.6 MHz ($L = 1200$ nH and parasitic capacitance $C_p \sim 0.4$ pF), a matching capacitor of $C_m = 39$ pF and

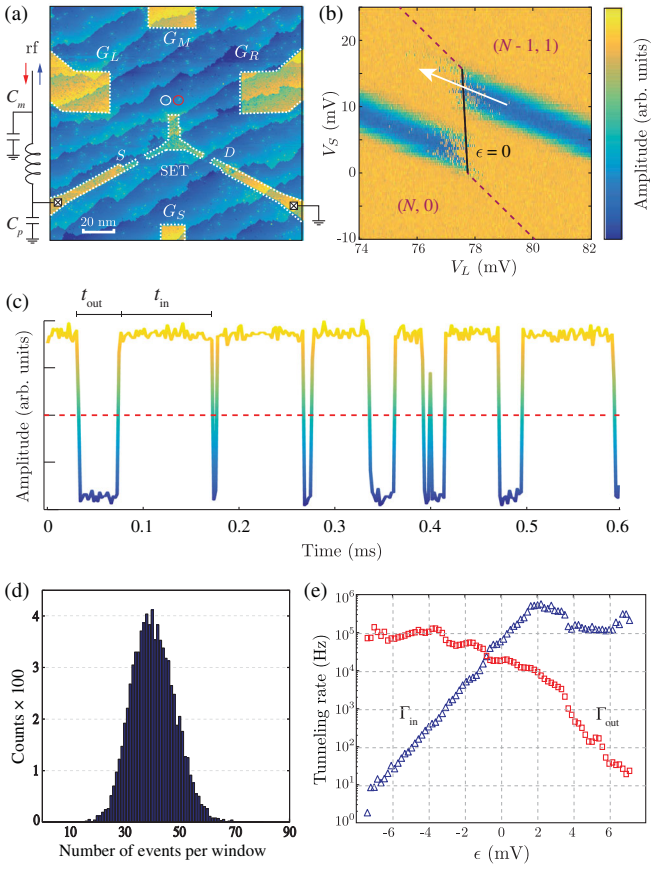

FIG. 1. Full counting statistics of a few-donor quantum dot coupled to an in-plane rf SET. (a) A STM micrograph of the device investigated. Two DDs are patterned in the device; however, in the paper, we study only the right DD (red circle). There are three control gates for the DDs $\{G_L, G_M, G_R\}$ and one for the rf SET, G_S. The rf-tank circuit is attached to the source contact, and the drain is grounded. The tank circuit is characterized by $L = 1200$ nH, a parasitic capacitance $C_p \sim 0.4$ pF, and a matching capacitor $C_m = 39$ pF. A variable attenuator is used to tune the rf power reaching the device. (b) An anticrossing between the DD and rf SET at $B = 0$ T in the reflected amplitude of the rf signal showing relative electron numbers on SET and DD (n_{SET},n_{DD}). The detuning axis ϵ is shown by the white arrow. (c) An illustrative RTS trace taken by measuring the reflected amplitude of the rf SET near $\epsilon = 0$ in (b). (d) The resulting distribution $p(n)$ after using FCS to analyze the RTS trace in (c) at $B = 0$ T. The histogram shows a mean of approximately 40 with a variance of approximately 20. The distribution is positively skewed, that is, SF > 0. (e) The measured tunnel rates as a function of detuning at $B = 0$ T showing the Fermi distribution about the Fermi level of the rf SET.

Q factor of approximately 150 attached to the source contact, while the drain contact is grounded [32]. The amplitude of the reflected signal is monitored throughout the experiment, and a variable attenuator is used to adjust the input rf power driving the SET. While two DDs of approximately 5 P each are patterned in the device, we concentrate on the right DD in this paper since we are interested only in the single-electron dynamics between the DD and rf SET. Figure 1(b) shows a charge transition between the DD and rf SET with the detuning ϵ between the DD and SET along the white arrow.

To acquire the RTS traces, we position the chemical potential of the DD such that an electron can tunnel to the rf SET. We then monitor the rf SET for 100 s before shifting the chemical potential along the detuning direction shown by the white arrow in Fig. 1(b) (see Appendix A for details of the FCS analysis). The reflected rf-amplitude RTS traces are digitized with a 500-kHz sample rate with an example trace shown in Fig. 1(c). The low level (blue) of the RTS trace corresponds to the DD having an extra electron, whereas the high level (yellow) indicates when an electron tunnels off the DD to the SET reservoir. We set a threshold level shown as a red dashed line in Fig. 1(c) that distinguishes between the DD charge states, 0 (yellow) and 1 (blue). The number of electrons on the SET and DD is given by (N_{SET}, N_{DD}) in the figure and do not represent absolute numbers since we do not deplete the DD for this experiment.

A. Random telegraph signal analysis

To encapsulate the complete dynamics of the system, we consider the system evolving under the Liouville equation, assuming the Born-Markov approximation,

$$\frac{d\rho}{dt} = \mathcal{L}\rho, \tag{1}$$

where ρ is the density operator, and $\mathcal{L}$ is the generator of the system, which includes both coherent and incoherent tunneling processes. The cumulants for a given generator $\mathcal{L}$ can be found by using FCS to analyze the RTS. Here, we use the recently proposed characteristic polynomial approach [30], which links the generator to the cumulants of the number distribution of tunnel events $p(n)$; see Fig 1(d) where the tunnel out events are used to generate the distribution. In addition, we extract the distribution of waiting times of the 0 and 1 states from which we can determine the tunnel rates as a function of detuning as shown in Fig. 1(e) at $B = 0$ T.

For degenerate spin states [$B = 0$ T; see Fig. 2(a)], the system has only two distinguishable states: $|0\rangle$ when there is no electron on the DD and $|1\rangle$ when there is one electron on the DD. The generator $\mathcal{L}$ in the basis $\{|0\rangle, |1\rangle\}$ contains the tunnel rates of the electron between the DD and reservoir,

$$\mathcal{L}_0 = \begin{pmatrix} -\Gamma_{\mathrm{in}} & \Gamma_{\mathrm{out}} \\ \Gamma_{\mathrm{in}} & -\Gamma_{\mathrm{out}} \end{pmatrix}, \tag{2}$$

where Γ_{in} (Γ_{out}) is the tunnel rate from the SET to DD (DD to SET) shown in the distribution of waiting times in Fig. 2(b). To perform FCS, we introduce a counting field ξ

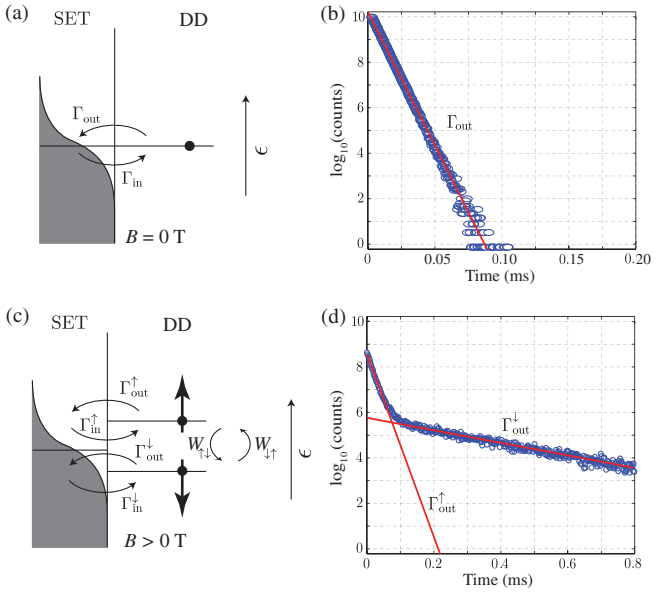

FIG. 2. The effect of an applied magnetic field to the distribution of waiting times. A schematic of the detuning and spin states $|\uparrow\rangle$ and $|\downarrow\rangle$ at (a) $B = 0$ T and (b) $B > 0$ T showing the individual tunnel rates between the DD and SET with thermal broadening. (c) At $B = 0$ T, the spin states are degenerate, and only a single exponential decay in the distribution of waiting times is observed. (d) At $B > 0$ T, the spin states are split by the Zeeman energy causing two distinct tunnel out rates of the DD to the rf SET. As a result, the distribution of waiting times shows a double exponential decay for $\Gamma^{\uparrow}_{out}$ and $\Gamma^{\downarrow}_{out}$.

over the transition that is measured by examining the RTS traces; see Fig. 1(c). The introduction of the counting field transforms $\mathcal{L}_0 \rightarrow \mathcal{L}_0^{\xi}$, which is given by

$$\mathcal{L}_0^{\xi} = \begin{pmatrix} -\Gamma_{in} & e^{\xi}\Gamma_{out} \\ \Gamma_{in} & -\Gamma_{out} \end{pmatrix}, \tag{3}$$

where the counting is performed over the tunnel out events of the DD to the rf SET ($|1\rangle \rightarrow |0\rangle$). The choice of tunnel in or out events does not affect the FCS analysis, and the same $p(n)$ can be obtained by counting over the tunnel in events from the rf SET to the DD.

To calculate the cumulants of $\mathcal{L}_0^{\xi}$, we use the recently proposed characteristic polynomial approach to counting statistics [30]. This method uses the characteristic polynomial $P^{\xi}(z) = \det(z\mathcal{I} - \mathcal{L}^{\xi})$ of the generator (where z is a placeholder variable, and $\mathcal{I}$ is the identity matrix) to find the cumulants rather than finding the smallest eigenvalue of the generator [19]. The notable benefit of the characteristic polynomial approach is that analytical expressions for the cumulants can always be obtained since it is not necessary to find the eigenvalues of the generator [the roots of $P^{\xi}(z)$] [30]. In addition, statistical tests of the system dimension can be derived, and the measured cumulants can be inverted to determine an unknown generator [30]. Therefore, the characteristic polynomial allows for more information to be gained from the counting statistics compared to the standard approach [19].

In general, the characteristic polynomial $P^{\xi}(z)$ is related to the cumulants of the generator through the total derivative of $P^{\xi}[\lambda(\xi)]$ with respect to the counting field ξ [30],

$$\left.\frac{d^l P^{\xi}[\lambda(\xi)]}{d\xi^l}\right|_{\xi=0} = 0, \qquad l \geq 1, \tag{4}$$

where $\lambda(\xi)$ is the smallest eigenvalue of the generator. Evaluating Eq. (4) for $l = \{1, 2, 3\}$ and taking into account the relations $\kappa_i = \partial_{\xi}^{i}\lambda(\xi)|_{\xi=0}$ and $\lambda(\xi)|_{\xi=0} = 0$, we can solve for the cumulants κ_1, κ_2, and κ_3 [30],

$$\kappa_1 = -\frac{a_0'}{a_1}, \tag{5}$$

$$\kappa_2 = -\frac{1}{a_1}(a_0' + 2a_1'\kappa_1 + 2a_2\kappa_1^2), \tag{6}$$

$$\kappa_3 = -\frac{1}{a_1}(a_0' + 3a_1'\kappa_1 + 6a_2\kappa_1^2 + 6a_3\kappa_1^3 + 3a_1'\kappa_2 + 6a_2\kappa_1\kappa_2), \tag{7}$$

where a_n is the nth coefficient of z in the characteristic polynomial. Similarly, a_n' is the derivative of the nth of z with respect to ξ in the limit that $\xi \rightarrow 0$. Using Eqs. (5)–(7), we can readily find the analytical expressions for the first three cumulants from the coefficients of the characteristic polynomial.

The characteristic polynomial of the $\mathcal{L}_0^{\xi}$ in the case of degenerate spin states has the form,

$$P_0^{\xi}(z) = z^2 + (\Gamma_{in} + \Gamma_{out})z + \Gamma_{out}\Gamma_{in}(1 - e^{\xi}). \tag{8}$$

Substituting in the coefficients of $P_0^{\xi}(z)$ gives

$$\kappa_1 = \frac{\Gamma_{in}\Gamma_{out}}{\Gamma_{in} + \Gamma_{out}}, \tag{9}$$

$$\kappa_2 = \kappa_1 \frac{\Gamma_{in}^2 + \Gamma_{out}^2}{(\Gamma_{in} + \Gamma_{out})^2}, \tag{10}$$

$$\kappa_3 = \kappa_1 \frac{\Gamma_{in}^4 - 2\Gamma_{in}^3\Gamma_{out} + 6\Gamma_{in}^2\Gamma_{out}^2 - 2\Gamma_{in}\Gamma_{out}^3 + \Gamma_{out}^4}{(\Gamma_{in} + \Gamma_{out})^4}. \tag{11}$$

For energy-selective electron spin readout, the electron Zeeman split-energy levels $|\uparrow\rangle$ and $|\downarrow\rangle$ must have an energy separation $g\mu_B B > k_B T$, where $g\mu_B B$ is the Zeeman energy for magnetic field strength B, and $k_B T$ is the thermal energy at temperature T. The spin-split levels are then positioned with the Fermi level of a reservoir between

them, such that only $|\uparrow\rangle$ can tunnel out and $|\downarrow\rangle$ can tunnel in. However, due to temperature broadening, there is a finite probability that the electrons can tunnel back and forth between the reservoir and DD indefinitely.

When a magnetic field is applied, the spin states become nondegenerate, and we must now consider a three-state system; see Fig. 2(c). In this case, each spin state has distinct dynamics due to their different chemical potential with respect to the Fermi level of the SET, resulting in different tunnel rates $\{\Gamma_{\rm in}^{\downarrow}, \Gamma_{\rm out}^{\downarrow}, \Gamma_{\rm in}^{\uparrow}, \Gamma_{\rm out}^{\uparrow}\}$ as well as interspin relaxation rates $W_{\uparrow\downarrow}$ and $W_{\downarrow\uparrow}$. This added complexity significantly changes the cumulants of the system, and, hence, six tunnel rates are now required to describe the DD SET tunneling. This change in the cumulants can be immediately seen by examining the distribution of waiting times in Fig. 2(d) where two exponential decays are observed corresponding to the individual spin tunnel rates. In the limit that the interspin relaxation rates are much smaller than the DD SET tunnel rates, κ_1 is given by

$$\kappa_1 = \frac{\Gamma_{\rm in}^{\downarrow}\Gamma_{\rm out}^{\uparrow}(\Gamma_{\rm in}^{\uparrow} + \Gamma_{\rm in}^{\downarrow})}{\Gamma_{\rm in}^{\downarrow}\Gamma_{\rm out}^{\uparrow} + \Gamma_{\rm out}^{\downarrow}(\Gamma_{\rm in}^{\uparrow} + \Gamma_{\rm out}^{\uparrow})}. \tag{12}$$

This limiting equation is the case for the most donor systems with long spin relaxation times $T_1 > 1$ s at $B = 2.5$ T. The higher-order cumulants can be calculated in an equivalent manner to the $B = 0$ T case; however, their general analytical form is too large to quote [33].

The normalized second cumulant known as the Fano factor (FF) defined as $\mathrm{FF} = \kappa_2/\kappa_1$ is a useful quantity when investigating the system dynamics since it gives information about the temporal distribution of the tunnel events. That is, for tunnel events that are evenly separated in time (antibunching), $\mathrm{FF} < 1$, and for tunnel events that are clustered with long periods of no tunneling (bunching), $\mathrm{FF} > 1$. We also make use of the normalized skewness, $\mathrm{SF} = \kappa_3/\kappa_1$. While FF must be positive, SF can range from $-\infty$ to ∞. For $\mathrm{SF} < 0$, $p(n)$ extends further in n values less than κ_1; that is, the distribution is negatively skewed. Conversely, for $\mathrm{SF} > 0$, $p(n)$ has more values larger than κ_1, meaning the distribution is now positively skewed. In particular, a Gaussian distribution is described by $\mathrm{SF} = 0$ or, more precisely, $\kappa_{i>2} = 0$. We make use of SF in Sec. III C to determine the lowest magnetic field where the spin states are distinguishable.

III. MAGNETIC FIELD DEPENDENCE

To fully understand the tunneling dynamics of the DD SET system, we consider three distinct magnetic field regimes—low ($g\mu_B B < k_B T$) and high ($g\mu_B B > k_B T$) magnetic field—where the system can be described by a two-state ($\{|0\rangle, |1\rangle\}$) and three-state ($\{|0\rangle, |\downarrow\rangle, |\uparrow\rangle\}$) system, respectively, and the intermediate magnetic field ($g\mu_B B \sim k_B T$) case. We then use a statistical test to determine the magnetic field for which the system can no longer be described by a two-state model.

A. Low magnetic field

First, we consider the system at $B = 0$ T for which the spin states are degenerate. The tunneling of the electrons produces a RTS trace such as shown in Fig. 1(c) corresponding to the two charge states of the DD, $|0\rangle$ (high level) and $|1\rangle$ (low level).

The shaded bands in Fig. 3(a) show the FF of the tunnel events of the DD to the SET ($\hat{\kappa}_i$ are cumulants determined from the experimental data; see Appendix A) as a function of detuning ϵ between the DD and rf SET [see arrow in Fig. 1(b)]. There is a single dip near $\epsilon = 0$ [position ②] that has a minimum of approximately 0.55. This is an indication of electron antibunching [22] in which the electron tunnel out events are evenly spaced out in time. This is due to the fermionic nature of the electron such that only one can occupy a specific DD energy level at a time. It is worth noting that the FF does not reach 0.5 since the tunnel rates are extremely sensitive at $\epsilon = 0$, and small electrical noise fluctuations can change them significantly. As a result, on average, the tunnel rates are not exactly equal at $\epsilon = 0$, and there is some additional variance in the counting statistics introduced from the noise in the system. The FF then approaches 1 for $\epsilon \ll 0$ [position ①] and $\epsilon \gg 0$ [position ③] where the electron becomes Coulomb blockaded and cannot tunnel between the DD and SET. The FF agrees very well with theoretical calculations (solid lines) where only an effective temperature is assumed, as is standard practice for a dc SET. For example, at -100 dB m, the effective power-broadened temperature is approximately 1.4 K (see Appendix B for details on the temperature calculation). Since the tunneling statistics can be described by a simple effective temperature broadening in the same manner as a dc SET, we conclude that the rf SET is suitable for single-shot electron spin readout. Note that below, we perform the same experiment with much lower rf-driving powers, and, hence, a lower power-broadened temperature.

Although the FF can distinguish between the overall behavior of the tunneling dynamics, to examine the temporal correlations of tunnel events, we make use of the second-order correlation function $g^{(2)}(t)$ [34],

$$g^{(2)}(t) = \frac{\langle\langle \mathcal{J} e^{\mathcal{L}t} \mathcal{J} \rangle\rangle}{\langle\langle \mathcal{J} \rangle\rangle^2}, \tag{13}$$

where $\mathcal{J} = d\mathcal{L}(\xi)/d\xi|_{\xi=0}$ is the jump operator for the counting field ξ, and $\langle\langle \ldots \rangle\rangle$ indicates the steady-state average. The $g^{(2)}(t)$ can be used to distinguish between antibunching [$g^{(2)}(t) < 1$] and bunching [$g^{(2)}(t) > 1$] tunnel events. Experimentally, $g^{(2)}(t)$ is calculated by building a histogram of the times t between every pair of tunnel out events in the RTS trace. We note by definition, $g^{(2)}(0) = 0$

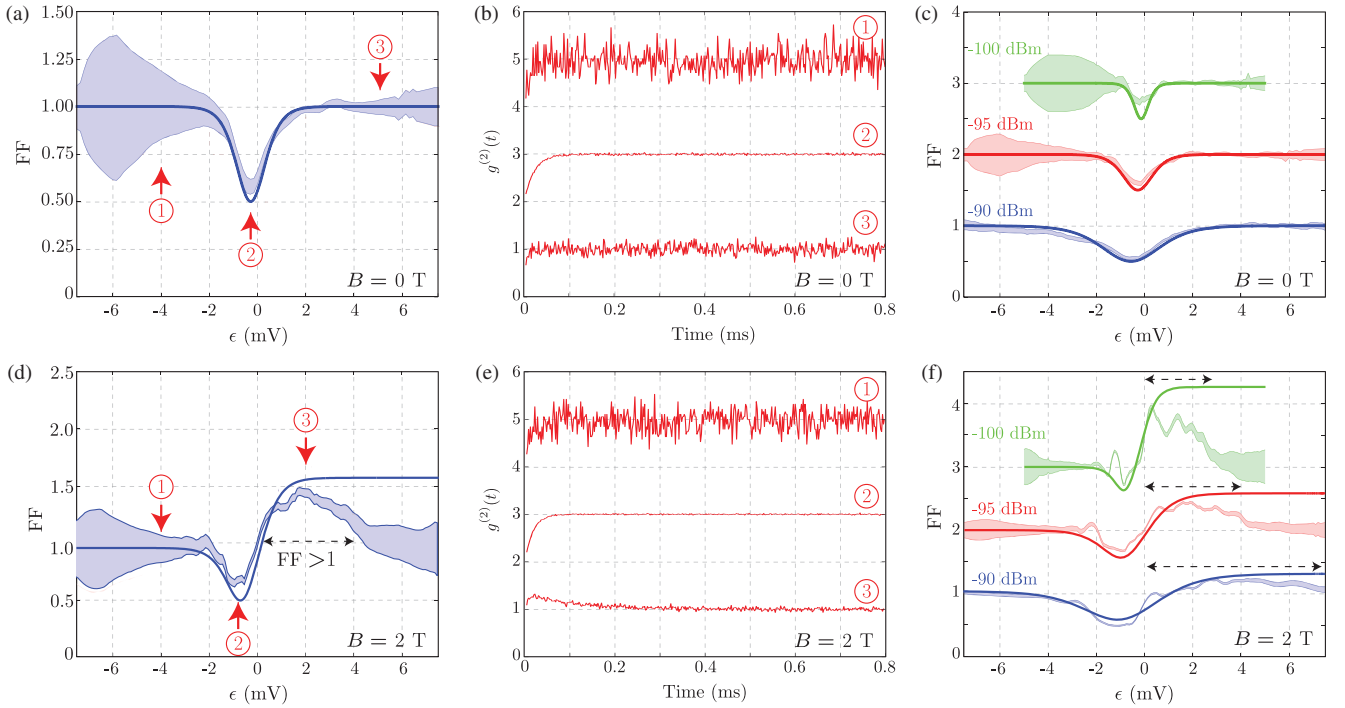

FIG. 3. Second-order correlation function and power dependence of the Fano factor as a function of detuning. (a) Fano factor $\mathrm{FF} = \hat{\kappa}_2/\hat{\kappa}_1$ as a function of detuning ϵ between the DD and rf SET at $B = 0$ T and −95 dB m. There is a dip to $\mathrm{FF} \sim 0.5$ near zero detuning, indicating antibunching of electrons tunneling between the DD and the rf SET. The shaded region is the confidence interval of the experimental data, and the solid line is a fit assuming a Fermi distribution of the SET. (b) Second-order correlation function $g^{(2)}(t)$ at the three different detuning positions (offset by 2) for $B = 0$ T labeled in (a). All detuning positions show antibunching $g^{(2)}(t) \leq 1$ confirming the FF measurement in (a). The dips near $t = 0$ for ① and ③ are due to the limited bandwidth of the rf SET. (c) The power dependence of the FF for three different rf powers (−90, −95, and −100 dB m) applied to the SET (offset by 1). As the power is increased, the FF broadens as the result of a larger effective electron temperature. (d) FF at $B = 2$ T. There is now a peak in the FF above 1, which indicates bunching of electron tunnel events due to the different tunnel rates between the Zeeman split-spin states. (e) $g^{(2)}(t)$ at three different detuning positions for $B = 2$ T (offset by 2). For position ②, antibunching is also observed as the $|\downarrow\rangle$ state is aligned with the rf SET Fermi level, and, therefore, electrons can tunnel back and forth to the SET. At position ③, there is clear evidence of bunching of electrons $g^{(2)}(t) > 1$, confirming the FF measurements in (d). Again, the sharp dip near $t = 0$ is due to the limited bandwidth of the rf SET. (f) The power dependence of FF at $B = 2$ T (offset by 1). The peak in the FF becomes less pronounced as rf power increases. This is a result of the increasing electron temperature since the height of the peak depends on the difference in the tunnel out rate between the $|\downarrow\rangle$ and $|\uparrow\rangle$ states. The width of the peak (dashed line) increases since there is a larger detuning range over which sufficient tunneling statistics can be obtained.

since electrons are fermions; that is, we cannot detect individual tunnel events that are not separated in time [34].

The second-order correlation function is shown in Fig. 3(b) at the three different detuning positions marked ①, ②, and ③ in Fig. 2(a). At $\epsilon \approx 0$ [point ②], $g^{(2)}(t) < 1$ for $t < 0.1$ ms indicating that electron antibunching is observed at these short time scales. For large detuning [① and ③] where the DD is in Coulomb blockade, $g^{(2)}(t) = 1$ since the tunnel events are not correlated in time. This confirms the observation of the FF dip in Fig. 3(a).

Finally, in this low field regime, we investigate the counting statistics as a function of the applied rf power to examine the effect of any artificial broadening due to rf driving of the SET. Any broadening due to excessive rf power is relevant when considering electron spin-readout fidelities, which are strongly reduced at high electron temperatures. Figure 3(c) shows the FF as a function of detuning for three rf powers. We observe that increased rf power broadens the FF dip, indicating that the higher power causes a higher effective temperature of the SET. However, it does not significantly affect the counting statistics since the tunneling dynamics can still be explained by the simple dc reservoir model (solid lines). Therefore, although the rf driving of the SET does not change the tunneling dynamics, the rf power needs to be chosen carefully as not to power broaden the SET which will ultimately decrease the electron spin-readout fidelity, in particular, as $k_B T \rightarrow g\mu_B B$.

B. High magnetic field

We now examine the high-magnetic-field case where the electron spin state can be read out since the spin-split levels are sufficiently distinct to allow spin-to-charge conversion

[35]. Therefore, it is important to characterize the dynamics of the nondegenerate spin states using the rf SET to determine any detrimental effects that may affect single-shot spin readout.

At large magnetic fields $g\mu_B B > k_B T$, the dynamics can no longer be explained by a two-level system. The Zeeman split levels now have their own dynamics, and the generator must describe a three-state system. The generator $\mathcal{L}_B$ in the basis $\{|0\rangle, |\downarrow\rangle, |\uparrow\rangle\}$ of the DD electron is given by

$$\mathcal{L}_B = \begin{pmatrix} -\Gamma_{\text{in}}^{\uparrow} - \Gamma_{\text{in}}^{\downarrow} & \Gamma_{\text{out}}^{\downarrow} & \Gamma_{\text{out}}^{\uparrow} \\ \Gamma_{\text{in}}^{\downarrow} & -\Gamma_{\text{out}}^{\downarrow} - W_{\downarrow\uparrow} & W_{\uparrow\downarrow} \\ \Gamma_{\text{in}}^{\uparrow} & W_{\downarrow\uparrow} & -\Gamma_{\text{out}}^{\uparrow} - W_{\uparrow\downarrow} \end{pmatrix}, \quad (14)$$

where Γ_n^i are the tunnel rates for the individual spin states in and out of the DD, and $W_{\uparrow\downarrow}$ ($W_{\downarrow\uparrow}$) is the relaxation rate from $|\uparrow\rangle \rightarrow |\downarrow\rangle$ ($|\downarrow\rangle \rightarrow |\uparrow\rangle$).

The measured FF as a function of detuning at $B = 2$ T is shown in Fig. 3(d). There is a dip near $\epsilon = 0$ [position ②] as seen in the low-magnetic-field case indicative of antibunching. The FF then rises above 1 ($\epsilon > 0$) for a length of detuning before returning to 1. This arises due to the bunching of the electron tunnel events due to the different tunnel rates of the Zeeman split states. The width in detuning for which FF > 1 shown by the dashed lines is related to the temperature of the system and Zeeman splitting of the spin states. The discrepancy between the theoretical curve and data at far positive detuning is due to the finite window size τ in our analysis. If $\tau \sim 1/\Gamma_n^i$, then FCS breaks down, and the number distribution cannot be described accurately. As a result, the distribution becomes Poissonian, $\kappa_{i>1} = \kappa_1$ and, hence, FF $\rightarrow 1$.

The detuning for which the FF rises above 1 shows where bunching of the $|\uparrow\rangle$ tunneling to the SET occurs. Here, the electron can tunnel back and forth to the SET; however, if $|\downarrow\rangle$ is loaded onto the DD, then the tunnel out rate to the SET is much slower [this is schematically shown in Fig. 1(c)]. This configuration results in periods of fast tunneling ($|\uparrow\rangle \leftrightarrow |0\rangle$) interspersed with periods of slow tunneling ($|\downarrow\rangle \leftrightarrow |0\rangle$). This extra spin state gives rise to the observed super-Poissonian (FF > 1) statistics in the counting statistics as it acts as a blocking state [17]. We can confirm the presence of a blocking state by looking at the second-order correlation function of the RTS trace shown in Fig. 3(e) for three different detuning positions. Near position ② where FF ≈ 0.6, two-state dynamics and antibunching of tunnel events are observed, confirmed by $g^{(2)}(t) < 1$. At the peak of the FF ≈ 1.5 [position ③], there is clear evidence of the bunching of the electrons for $t < 0.2$ ms since $g^{(2)}(t) > 1$.

We again examine the rf-power dependence on the FCS at high magnetic field in Fig. 3(f). The region where FF > 1 widens in detuning and decreases in amplitude at larger powers since the effective temperature of the system increases, causing the tunnel rates of the two spin states to become more similar. As before, the dynamics of the system can be described by considering only an effective temperature broadening, indicating that the rf driving does not give rise to any new dynamics in the system. This is most likely due to the much slower tunnel rates (approximately 50 kHz) compared to the rf-driving frequency (228.6 MHz).

C. Intermediate magnetic fields

The condition FF > 1 gives an indication of where the two-state (degenerate spin) model cannot be used to describe the system [30]. In Fig. 4(a), we plot the FF as a function of magnetic field and detuning. The FF peak increases in magnitude and width as the magnetic field is increased, showing that the magnetic field has a direct effect on the system dynamics. To investigate the transition from a two-state to a three-state system, we measure the normalized skewness SF $= \kappa_3/\kappa_1$ at magnetic field values in the intermediate regime $g\mu_B B \sim k_B T$ or $0 < B < 1$ T.

The two-state system has only two independent cumulants, κ_1 and κ_2; that is, any cumulant $\kappa_{i>2}$ can be written as a function of the preceding cumulants which allows us to determine a statistical test of the system dimension [30]. In this section, we test the hypothesis that the DD and rf SET electron system is classical (in the sense that the Hamiltonian contains only nonzero diagonal elements) and of dimension, $M = 2$. To this end, we have to measure the first three cumulants $\{\hat{\kappa}_1, \hat{\kappa}_2, \hat{\kappa}_3\}$. Using the measured first two cumulants $\hat{\kappa}_1$, $\hat{\kappa}_2$, we calculate what the third cumulant *would* be for a two-state system,

$$\kappa_3 = \hat{\kappa}_1 + 3\hat{\kappa}_2\left(\frac{\hat{\kappa}_2}{\hat{\kappa}_1} - 1\right). \quad (15)$$

If $\kappa_3 \neq \hat{\kappa}_3$, then the hypothesis that the system has a dimension $M = 2$ must be rejected and, hence, cannot be described by a two-dimensional generator, which, in our case, is $\mathcal{L}_0$.

To investigate the two-state hypothesis, we first examine the detuning dependence of $\hat{\kappa}_3$ and κ_3 at $B = 1.5$ T in Fig. 4(b). Importantly, the detuning dependence on $\hat{\kappa}_3$ and κ_3 shows that the experiment and calculated cumulant disagree only where FF > 1 between $\epsilon \approx 0$ mV and $\epsilon \approx 4$ mV. The difference between κ_3 and $\hat{\kappa}_3$ occurs where the FF > 1 as this corresponds to where $|\uparrow\rangle$ is above the Fermi level of SET, and $|\downarrow\rangle$ is below the Fermi level giving different tunnel rates to the SET. Therefore, the three-state model must be used.

To examine the magnetic field dependence, we take a cut through the SF at $\epsilon = 1.5$ mV shown in Fig. 4(c). The transition from the two-state to three-state system, that is, where $\kappa_3 \neq \hat{\kappa}_3$ occurs around $B_{\text{tran}} = 0.4 \pm 0.1$ T. This magnetic field strength B_{tran} represents the point where the thermal broadening of the rf SET causes the individual

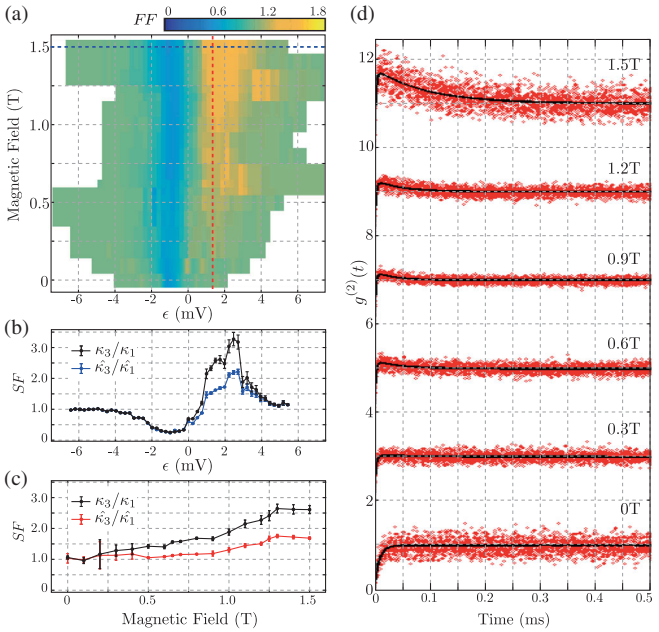

FIG. 4. Transition from a two- to a three-state system. (a) The magnetic field B dependence of the measured Fano factor $\mathrm{FF} = \hat{\kappa}_2/\hat{\kappa}_1$. The peak can be seen to emerge at low magnetic fields and increase in height as B increases. The data are aligned such that the minima in the Fano factors for different B values are at the same detuning value. (b) The detuning dependence of the calculated and measured normalized skewness SF; κ_3/κ_1 and $\hat{\kappa}_3/\hat{\kappa}_1$ at $B = 1.5$ T [blue dashed line in (a)]. The calculated and measured cumulants differ only around the peak in the Fano factor, indicating that the two-state model must be rejected in this detuning regime. (c) κ_3/κ_1 and $\hat{\kappa}_3/\hat{\kappa}_1$ as a function of B along the detuning position indicated in (a) at $\epsilon = 1.5$ mV (red dashed line). The cumulants become significantly different above $B = 0.4$ T, showing that the three-state model is required above this magnetic field strength. (d) Selected $g^{(2)}(t)$ traces for different B fields from 0 to 1.5 T at $\epsilon = 1.5$ mV (offset by 2). As the magnetic field is increased, the bunching of electrons $g^{(2)}(t) > 1$ becomes more prominent since the ratio of the spin-state tunnel rates difference becomes larger. The extent in time of the $g^{(2)}(t) > 1$ region also increases, again, indicative that the ratio between the two-spin-state tunnel rates becomes larger as the magnetic field is increased. The solid lines are fits to the data using Eq. (13).

spin-state $|\uparrow\rangle$ and $|\downarrow\rangle$ tunnel rates to become indistinguishable [36].

Finally, we plot $g^{(2)}(t)$ in Fig. 4(d) for various magnetic field strengths along the same detuning as in Fig. 4(c). As the magnetic field is increased, the bunching of tunneling out events $[g^{(2)}(t) > 1]$ becomes more prominent as the difference in energy between the spin-up and spin-down states increases. This is because the blocking spin-down state causes larger periods of no tunneling. Below B_{tran}, the signature of bunching, that is, $g^{(2)}(t) > 1$ disappears, and only antibunching of electrons can be observed $g^{(2)}(t) < 1$.

IV. DETERMINING OPTIMAL SINGLE-SPIN READOUT

For optimal spin readout, the electron temperature should be as low as possible to maximize spin-to-charge conversion, which relies on sufficiently different Γ^i_{out} for spin-up and -down. The next step is to examine what effect the rf-driving field has on the fidelity of single-shot electron spin readout.

Electron spin-readout fidelities are separated into two processes: electrical visibility and spin-to-charge conversion visibility. Electrical visibility represents the probability of registering a tunnel event (a blip in the detector response) and is governed predominately by the SNR, readout time, and measurement bandwidth of the detector. The spin-to-charge conversion visibility indicates how well the detector is able to distinguish between a tunnel event that is $|\uparrow\rangle$ or $|\downarrow\rangle$ and depends on the relative tunnel out times of the individual spin states [35]. We want the tunnel rate of $|\uparrow\rangle \rightarrow |0\rangle$ to be much greater than $|\downarrow\rangle \rightarrow |0\rangle$. Therefore, the spin states are positioned such that the $|\uparrow\rangle$ chemical potential is above the Fermi level of the SET and that $|\downarrow\rangle$ is below the Fermi level. Since we measure the tunnel rates as a function of detuning, we can optimize the readout fidelity over the detuning range and rf power for a given magnetic field value. An explanation of the various parameters involved in the spin-readout fidelity calculation is given in Appendix C.

A. Optimization of readout time

In Fig. 5(a), we plot the measured tunnel rates obtained from the waiting time distribution of the RTS trace by fitting a double exponential function which gives distinct tunnel out rates (Appendix B) for $|\uparrow\rangle$ (higher tunnel rate, red squares) and $|\downarrow\rangle$ (lower tunnel rate, blue circles). The tunnel in time corresponds to $\Gamma_{\mathrm{in}} = \Gamma^{\downarrow}_{\mathrm{in}} + \Gamma^{\uparrow}_{\mathrm{in}}$ and shows only the sum of the two times and, therefore, only a single exponential can be fit to the data (green triangles). The solid lines are fits to the data using a Fermi-Dirac distribution [9,35]. The optimum point for spin-to-charge conversion is where the ratio $\Gamma_{\mathrm{ratio}} = \Gamma^{\uparrow}_{\mathrm{out}}/\Gamma^{\downarrow}_{\mathrm{out}}$ is maximized. From Fig. 5(a), we can see that Γ_{ratio} does not vary over the detuning range $\epsilon > 2$ mV, implying that any point in this region will give the optimal spin-to-charge conversion fidelity. However, the optimum readout time will be faster as $\Gamma^{\uparrow}_{\mathrm{out}}$ becomes faster (moving towards negative detuning), meaning that the readout time can be tuned over many orders of magnitude depending on the position in detuning while maintaining the same spin-to-charge conversion fidelity. Interestingly, the detuning point that gives the fastest readout while maintaining the highest spin-to-charge conversion occurs at the peak of the FF denoted by the black arrow in Fig. 3(d), which at $B = 2$ T corresponds to approximately 2 mV. What this means is that by measuring

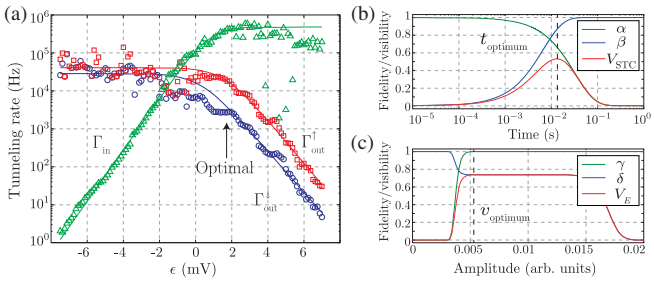

FIG. 5. Individual spin tunnel rates for spin readout. (a) Individual tunnel rates as a function of detuning ϵ at $B = 2$ T. Two tunnel rates can be observed in the regime where FF > 1, which we assign as $\Gamma^{\uparrow}_{out}$ (red squares) and $\Gamma^{\downarrow}_{out}$ (blue circles). A single tunnel in rate is measured since it is the sum of both the individual spin tunnel rates (green triangles). The solid lines are fits to the data using a Fermi-Dirac distribution. Using the data of the tunnel times as well as measuring the signal-to-noise ratio at different powers, we can perform a spin-readout fidelity analysis. (b) The spin-to-charge conversion visibility (red) as well as fidelities α (blue) and β (green) as a function of readout time. (c) The electrical fidelities γ (green) and δ (blue) as well as the electrical visibility (red) as a function of readout threshold. The maximum of these two plots is used to the obtain the optimum readout time and threshold value (t_{optimum} and v_{optimum}).

the FF as a function of detuning, the optimal readout position can be easily found from max[FF].

B. Optimization of rf power

Using the data from Fig. 5(a), we calculate the spin-to-charge conversion visibility ($V_{\mathrm{STC}} = \alpha + \beta - 1$) and the electrical visibility ($V_E = \gamma + \delta - 1$) in Figs. 5(b) and 5(c), which are used to obtain the electron spin-readout fidelity. This type of analysis has been reported before [35] and can be used to directly obtain the optimum readout time [Fig. 5(b)] and the optimal threshold for the tunnel event [Fig. 5(c)]. We now use the same methods to find the optimum spin-readout fidelity for different rf powers.

At higher rf powers, the effective temperature of the system increases. This is confirmed in Fig. 6(a), where we show the structure of the rf SET response across the charge transition with the DD. The higher effective temperature reduces the spin-to-charge conversion fidelity since the $|\uparrow\rangle$ and $|\downarrow\rangle$ tunnel events become less distinguishable. In Fig. 6(b), we show that as the applied rf power increases, the SNR also increases, which gives better electrical fidelity. However, there is a trade-off since the tunnel out times of spin-up and -down become more similar as the effective temperature increases. The electrical visibility has three distinct regimes. For small rf power, the SNR becomes too small to accurately register any tunnel event (red region). In the intermediate regime (green), the visibility reaches a maximum and slowly decreases as more rf power is applied to the rf SET. The decrease is due to the tunnel out rates becoming too similar. This means the

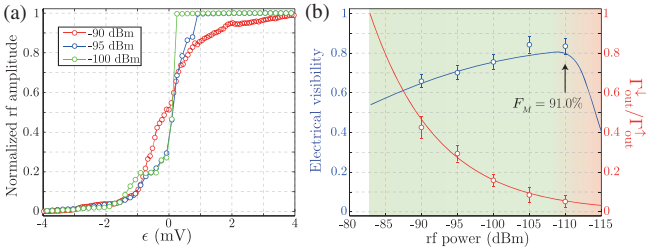

FIG. 6. The effect of rf power on spin-readout fidelity. (a) The edge of the SET rf-amplitude response across the DD anticrossing line. As the rf power is increased, the density of states in the SET broadens in detuning. (b) The calculated electrical visibility (blue) and tunnel rate ratio $\Gamma^{\downarrow}_{out}/\Gamma^{\uparrow}_{out}$ (red) as a function of rf power to the SET. The data points show the measured values in the experiment, and the solid lines are theoretical calculations using parameters obtained from the experiment. There is an optimum rf power for electron spin readout, which we calculate here to be $V_E = 84.2\%$, which, when combined with the spin-to-charge conversion analysis, gives a predicted measurement fidelity $F_M = 91.0\%$ at -110 dB m.

optimum readout time (calculated from spin-to-charge conversion) becomes much shorter, and a large number of $|\uparrow\rangle$ tunnel events are missed [35]. When the ratio of the tunnel rates becomes 1 (large rf power), then spin readout becomes impossible since the tunnel events are indistinguishable between $|\uparrow\rangle$ and $|\downarrow\rangle$ (white region). Therefore, there is an optimum power for spin readout, which for the device measured here is -110 dB m (effective temperature of approximately 0.8 K), which gives a predicted measurement fidelity of $F_M = (\alpha\gamma + \beta\delta)/2 = 91.0\%$ [35].

The electrical fidelity in this device is limited by the fast $\Gamma^{\downarrow}_{in} \approx 250$ kHz, which approaches the measurement bandwidth of our data acquisition device. This means some current blips go undetected by the charge sensor. In this work, the SNR is large enough to clearly distinguish between the two states (approximately 40 at -90 dB m), and in the future, the tunnel rates can be easily decreased by having the DD slightly farther away from the rf SET.

V. DISCUSSION

We investigate the full counting statistics of a single DD coupled to a rf SET for single-shot electron spin readout. FCS can be used as a tool for probing the system dynamics and elucidating the optimal conditions to maximize electron spin-readout fidelities. We show by studying the tunneling statistics of electrons that the rf SET can be used to perform single-shot spin readout of electrons.

We examine the spin-readout fidelities by varying the rf power of the SET and show that there is a clear optimal power that is a compromise between power broadening and SNR. We show that by simply measuring the FF as a function of the detuning between the DD and SET, the optimal readout position can be easily found from its maximum value. For this device, we calculate a readout

fidelity of 91.0% and predict that the rf SET can be used as a charge sensor with fault-tolerant single-shot spin-readout fidelities if the tunnel times of the DD to the rf SET are increased. In summary, we show that by directly coupling a DD to a rf SET and measuring the tunneling statistics, we can optimize the readout fidelities to allow for fault-tolerant single-shot spin readout.

ACKNOWLEDGMENTS

We thank M. Bruderer for enlightening discussions. This research is conducted by the Australian Research Council Centre of Excellence for Quantum Computation and Communication Technology (Project No. CE110001027) and the U.S. National Security Agency and U.S. Army Research Office (Contract No. W911NF-08-1-0527). M. Y. S. acknowledges an ARC Laureate Fellowship.

APPENDIX A: CALCULATION OF CUMULANTS FROM RTS TRACES

In this section, we describe how the RTS traces can be analyzed to obtain the cumulants of the distribution $p(n)$ using FCS. We position the voltage levels on the gates such that the electron can tunnel between the rf SET and DD. We then wait at this position for $\tau_M = 100$ s while monitoring the reflected amplitude of the SET. The RTS traces are then sectioned into consecutive windows of a length $\tau = 10$ ms for a total of 10 000 windows. The number of tunnel outs, that is, the number of times the RTS traces goes from a low value to a high value [see Fig. 1(c)] per window, is then binned into a histogram over the whole RTS trace. An example of the resulting histogram of $p(n)$ is shown in Fig. 1(d).

The cumulants of the $p(n)$ can be calculated by first calculating the moments of the distribution. The moments μ_i of $p(n)$ are found using

$$\mu_i = E[p(n)^i], \tag{A1}$$

where $E[\cdot]$ represents the expectation value (mean) of the distribution. The cumulants can then be found from the recursion formula,

$$\kappa_i = \mu_i - \sum_{j=1}^{i-1} \frac{(i-1)!}{(j-1)!(i-j)!} \kappa_j \mu_{i-j}. \tag{A2}$$

The next RTS trace is then taken by shifting the voltages on the gates along the detuning line shown by the white line in Fig. 1(b) and performing the same analysis as above. The distribution of waiting times is calculated from each measured t_{in} and t_{out} in Fig. 1(c) and then binned into a histogram.

APPENDIX B: TEMPERATURE ESTIMATIONS

The temperature estimations in the main text are found by fitting both the individual cumulants from the FCS analysis and the relative magnitude of the spin tunnel out rates as a function of detuning. The temperature can be found by using the relative magnitude of the tunnel rates if the Zeeman energy $E_z = g\mu_B B$ of the electron spin states is known. The tunnel out rates $\Gamma_{\text{out}}^{\downarrow}$ and $\Gamma_{\text{out}}^{\uparrow}$ follow Fermi distributions about the Fermi level of the reservoir,

$$\Gamma_{\text{out}}^{\downarrow} = [1 - f(\epsilon - E_z/2)]\Gamma_{\text{out}}, \tag{B1}$$

$$\Gamma_{\text{out}}^{\uparrow} = [1 - f(\epsilon + E_z/2)]\Gamma_{\text{out}}, \tag{B2}$$

where Γ_{out} is the maximum tunnel rate. Therefore, the relative magnitude between the two tunnel out rates is

$$\frac{\Gamma_{\text{out}}^{\uparrow}}{\Gamma_{\text{out}}^{\downarrow}} = \frac{1 - f(\epsilon + E_z/2)}{1 - f(\epsilon - E_z/2)}. \tag{B3}$$

At far positive detuning when $f(\epsilon + E_z/2) < 1$, Eq. (B3) is approximately independent of detuning and is given by the ratio E_z to $k_B T$. That is,

$$\lim_{\epsilon \to \infty} \frac{\Gamma_{\text{out}}^{\uparrow}}{\Gamma_{\text{out}}^{\downarrow}} = \exp\left(\frac{E_z}{k_B T}\right), \tag{B4}$$

such that, after inverting,

$$T = \frac{E_z}{k_B(\ln \Gamma_{\text{out}}^{\uparrow} - \ln \Gamma_{\text{out}}^{\downarrow})}. \tag{B5}$$

The temperature obtained using this method shows good agreement to the cumulants obtained using FCS, and, as such, is used to estimate the temperature of the system. At far positive detuning $\Gamma_{\text{out}}^{\uparrow}/\Gamma_{\text{out}}^{\downarrow} \approx 7$, which gives $T = 1.4 \pm 0.2$ K for -100 dB m (-95 dB m is $T = 2.3 \pm 0.3$ K and -90 dB m is $T = 3.1 \pm 0.4$ K).

APPENDIX C: SINGLE-SPIN-READOUT PARAMETERS

The electrical visibility is how well the blip in the detector response can be resolved. It is parametrized by two fidelities γ and δ that correspond to the distributions of the spin-down $N_{\downarrow}$ and spin-up state $N_{\uparrow}$,

$$\gamma = 1 - \int_{-\infty}^{v} N_{\downarrow} dV, \tag{C1}$$

$$\delta = 1 - \int_{v}^{\infty} N_{\uparrow} dV. \tag{C2}$$

Here, $N_\downarrow$ is the distribution of the readout trace when there is no blip and $N_\uparrow$ when there is a blip present, and V is the reflected rf amplitude. The optimal threshold voltage v_{optimum} is the value that maximizes the separation between the two distributions [35]. This optimum threshold can be conveniently calculated by maximizing the electrical visibility,

$$V_E = \gamma + \delta - 1. \tag{C3}$$

The state-to-charge conversion visibility is calculated by considering a rate equation model of the single-electron tunneling to the SET. The two parameters that are used to maximize the probability that the electron tunneling to the SET is a spin-up are α and β,

$$\alpha = e^{-[t/t^0_{\text{out}}]}, \tag{C4}$$

$$\beta = \frac{1}{T_{\text{out}}}[(1 - e^{-[t/t^0_{\text{out}}]})t^0_{\text{out}}t^1_{\text{out}} + (e^{-[(T_1+t^1_{\text{out}})/(t^1_{\text{out}}T_1)]t} - 1)T_1(t^1_{\text{out}} - t^0_{\text{out}})], \tag{C5}$$

where $T_{\text{out}} = T_1(t^0_{\text{out}} - t^1_{\text{out}}) + t^0_{\text{out}}t^1_{\text{out}}$. The fidelity α is the probability that the spin-down electron has not tunneled to the SET, and β is the probability that the spin-up electron has tunneled to the SET [35]. The optimal readout time t_{optimum} is the time that maximizes these two fidelities. This can be found by maximizing the state-to-charge conversion visibility,

$$V_{\text{STC}} = \alpha + \beta - 1. \tag{C6}$$

Finally, we define the measurement fidelity as the average probability of correctly identifying the spin-down and spin-up states. This is given by

$$F_M = \frac{F_\downarrow + F_\uparrow}{2} = \frac{\alpha\gamma + \beta\delta}{2} \tag{C7}$$

to take into account the effect of the state-to-charge conversion and electrical visibility.

[1] C. D. Hill, E. Peretz, S. J. Hile, M. G. House, M. Fuechsle, S. Rogge, M. Y. Simmons, and L. C. L. Hollenberg, A surface code quantum computer in silicon, Sci. Adv. **1**, e1500707 (2015).

[2] J. O'Gorman, N. H. Nickerson, P. Ross, J. J. L. Morton, and S. C. Benjamin, A silicon-based surface code quantum computer, npj Quantum Inf. **2**, 15019 (2016).

[3] R. G. Knobel and A. N. Cleland, Nanometre-scale displacement sensing using a single electron transistor, Nature (London) **424**, 291 (2003).

[4] T. Kambara, T. Kodera, Y. Arakawa, and S. Oda, Dual function of single electron transistor coupled with double quantum dot: Gating and charge sensing, Jpn. J. Appl. Phys. **52**, 04CJ01 (2013).

[5] F. A. Zwanenburg, A. S. Dzurak, A. Morello, M. Y. Simmons, L. C. L. Hollenberg, G. Klimeck, S. Rogge, S. N. Coppersmith, and M. A. Eriksson, Silicon quantum electronics, Rev. Mod. Phys. **85**, 961 (2013).

[6] C. Barthel, M. Kjærgaard, J. Medford, M. Stopa, C. M. Marcus, M. P. Hanson, and A. C. Gossard, Fast sensing of double-dot charge arrangement and spin state with a radio-frequency sensor quantum dot, Phys. Rev. B **81**, 161308 (2010).

[7] T. A. Baart, M. Shafiei, T. Fujita, C. Reichl, W. Wegscheider, and L. M. K. Vandersypen, Single-spin CCD, Nat. Nanotechnol. **11**, 330 (2016).

[8] T. F. Watson, B. Weber, M. G. House, H. Büch, and M. Y. Simmons, High-Fidelity Rapid Initialization and Readout of an Electron Spin via the Single Donor D^- Charge State, Phys. Rev. Lett. **115**, 166806 (2015).

[9] A. Morello, J. J. Pla, F. A. Zwanenburg, K. W. Chan, K. Y. Tan, H. Huebl, M. Mottonen, C. D. Nugroho, J. A. van Donkelaar, A. D. C. Alves, D. N. Jamieson, C. C. Escott, L. C. L. Hollenberg, R. G. Clark, and A. S. Dzurak, Single-shot readout of an electron spin in silicon, Nature (London) **467**, 687 (2010).

[10] R. J. Schoelkopf, P. Wahlgren, A. A. Kozhevnikov, P. Delsing, and D. E. Prober, The radio-frequency single-electron transistor (RF-SET): A fast and ultrasensitive electrometer, Science **280**, 1238 (1998).

[11] A. N. Korotkov and M. A. Paalanen, Charge sensitivity of radio frequency single-electron transistor, Appl. Phys. Lett. **74**, 4052 (1999).

[12] T. M. Buehler, D. J. Reilly, R. P. Starrett, A. D. Greentree, A. R. Hamilton, A. S. Dzurak, and R. G. Clark, Single-shot readout with the radio-frequency single-electron transistor in the presence of charge noise, Appl. Phys. Lett. **86**, 143117 (2005).

[13] S. J. Hile, M. G. House, E. Peretz, J. Vanduijn, D. Widmann, T. Kobayashi, S. Rogge, and M. Y. Simmons, Radio frequency reflectometry and charge sensing of a precision placed donor in silicon, Appl. Phys. Lett. **107**, 093504 (2015).

[14] J. M. Elzermaen, R. Hanson, L. H. Willems van Beveren, B. Witkamp, L. M. K. Vandersypen, and L. P. Kouwenhoven, Single-shot read-out of an individual electron spin in a quantum dot, Nature (London) **430**, 431 (2004).

[15] W. Lu, Z. Ji, L. Pfeiffer, K. W. West, and A. J. Rimberg, Real-time detection of electron tunnelling in a quantum dot, Nature (London) **423**, 422 (2003).

[16] R. Hanson, L. P. Kouwenhoven, J. R. Petta, S. Tarucha, and L. M. K. Vandersypen, Spins in few-electron quantum dots, Rev. Mod. Phys. **79**, 1217 (2007).

[17] K. Kaasbjerg and W. Belzig, Full counting statistics and shot noise of cotunneling in quantum dots and single-molecule transistors, Phys. Rev. B **91**, 235413 (2015).

[18] M. A. Broome, S. K. Gorman, J. G. Keizer, T. F. Watson, S. J. Hile, W. J. Baker, and M. Y. Simmons, Mapping the chemical potential landscape of a triple quantum dot, Phys. Rev. B **94**, 054314 (2016).

[19] D. A. Bagrets and Y. V. Nazarov, Full counting statistics of charge transfer in Coulomb blockade systems, Phys. Rev. B **67**, 085316 (2003).

[20] Y. V. Nazarov and M. Kindermann, Full counting statistics of a general quantum mechanical variable, Euro. Phys. J. B **35**, 413 (2003).

[21] L. D. Contreras-Pulido, M. Bruderer, S. F. Huelga, and M. B. Plenio, Dephasing-assisted transport in linear triple quantum dots, New J. Phys. **16**, 113061 (2014).

[22] S. Gustavsson, R. Leturcq, B. Simovic, R. Schieser, T. Ihn, P. Studerus, K. Ensslin, D. C. Driscoll, and A. C. Gossard, Counting Statistics of Single Electron Transport in a Quantum Dot, Phys. Rev. Lett. **96**, 076605 (2006).

[23] F. Hohls, N. Maire, C. Fricke, M. C. Rogge, and R. J. Haug, Shot noise and electron counting measurements on coupled quantum dot systems, J. Phys. Condens. Matter **20**, 454204 (2008).

[24] C. Flindt, T. Novotný, A. Braggio, M. Sassetti, and A.-P. Jauho, Counting Statistics of Non-Markovian Quantum Stochastic Processes, Phys. Rev. Lett. **100**, 150601 (2008).

[25] C. Flindt, C. Fricke, F. Hohls, T. Novotný, K. Netocny, T. Brandes, and R. J. Haug, Universal oscillations in counting statistics, Proc. Natl. Acad. Sci. U.S.A. **106**, 10116 (2009).

[26] C. Flindt, T. Novotný, A. Braggio, and A.-P. Jauho, Counting statistics of transport through Coulomb blockade nanostructures: High-order cumulants and non-Markovian effects, Phys. Rev. B **82**, 155407 (2010).

[27] A. Braggio, J. König, and R. Fazio, Full Counting Statistics in Strongly Interacting Systems: Non-Markovian Effects, Phys. Rev. Lett. **96**, 026805 (2006).

[28] C. Fricke, F. Hohls, N. Sethubalasubramanian, L. Fricke, and R. J. Haug, High-order cumulants in the counting statistics of asymmetric quantum dots, Appl. Phys. Lett. **96**, 202103 (2010).

[29] Z. Wang, H. Xue, N. Xue, and J.-Q. Liang, Full counting statistics of transport electrons through a two-level quantum dot with spin-orbit coupling, Ann. Phys. (Amsterdam) **353**, 9 (2015).

[30] M. Bruderer, L. D. Contreras-Pulido, M. Thaller, L. Sironi, D. Obreschkow, and M. B. Plenio, Inverse counting statistics for stochastic and open quantum systems: The characteristic polynomial approach, New J. Phys. **16**, 033030 (2014).

[31] M. Y. Simmons, F. J. Ruess, K. E. J. Roh, W. Pok, T. Hallam, M. J. Butcher, T. C. G. Reusch, G. Scappucci, A. R. Hamilton, and L. Oberbeck, Atomic-scale silicon device fabrication, Int. J. Nanotechnology **5**, 352 (2008).

[32] M. G. House, I. Bartlett, P. Pakkiam, M. Koch, E. Peretz, J. van der Heijden, T. Kobayashi, S. Rogge, and M. Y. Simmons, High-Sensitivity Charge Detection with a Single-Lead Quantum Dot for Scalable Quantum Computation, Phys. Rev. Applied **6**, 044016 (2016).

[33] W. Belzig, Full counting statistics of super-Poissonian shot noise in multilevel quantum dots, Phys. Rev. B **71**, 161301 (2005).

[34] C. Emary, C. Pöltl, A. Carmele, J. Kabuss, A. Knorr, and T. Brandes, Bunching and antibunching in electronic transport, Phys. Rev. B **85**, 165417 (2012).

[35] H. Büch, S. Mahapatra, R. Rahman, A. Morello, and M. Y. Simmons, Spin readout and addressability of phosphorous-donor clusters in silicon, Nat. Commun. **4**, 2017 (2013).

[36] M. G. House, M. Xiao, G. Guo, H. Li, G. Cao, M. M. Rosenthal, and H. Jiang, Detection and Measurement of Spin-Dependent Dynamics in Random Telegraph Signals, Phys. Rev. Lett. **111**, 126803 (2013).